



CHORUS

This is the accepted manuscript made available via CHORUS. The article has been published as:

Parallel Heat Flux from Low to High Parallel Temperature along a Magnetic Field Line

Zehua Guo and Xian-Zhu Tang

Phys. Rev. Lett. **108**, 165005 — Published 20 April 2012

DOI: [10.1103/PhysRevLett.108.165005](https://doi.org/10.1103/PhysRevLett.108.165005)

A parallel heat flux from low to high parallel temperature along a magnetic field line

Zehua Guo and Xian-Zhu Tang

Theoretical Division, Los Alamos National Laboratory, Los Alamos, NM 87545

(Dated: February 28, 2012)

In a long mean-free-path plasma where temperature anisotropy can be sustained, the parallel heat flux has two components with one associated with the parallel thermal energy and the other the perpendicular thermal energy. In a kinetic simulation with magnetic flux expansion toward an absorbing boundary, the parallel heat flux of the parallel thermal energy is found to flow from low to high parallel temperature region. This unusual behavior is understood with the help of an analytical calculation of the drift-kinetic model using the same upstream source in the simulation.

PACS numbers: 52.55.Dy, 52.25.Fi, 52.25.Dg

The plasma heat flux is the third-order moment of the species distribution function $f(\mathbf{x}, \mathbf{v})$, $\mathbf{q} = \int m\mathbf{v}^2 \mathbf{w} f d^3\mathbf{v}$, with $\mathbf{w} = \mathbf{v} - \mathbf{u}$ the particle fluctuation velocity and \mathbf{u} the plasma flow velocity. In a magnetized plasma, the perpendicular heat flux across magnetic field lines is greatly reduced. The ratio between parallel and perpendicular heat fluxes, $\mathbf{q}_{\parallel} = \int m\mathbf{v}^2 \mathbf{w}_{\parallel} f d^3\mathbf{v}$ with $\mathbf{w}_{\parallel} \equiv (\mathbf{w} \cdot \mathbf{b})\mathbf{b}$ and $\mathbf{b} \equiv \mathbf{B}/\|\mathbf{B}\|$, $\mathbf{q}_{\perp} = \int m\mathbf{v}^2 \mathbf{w}_{\perp} f d^3\mathbf{v}$ with $\mathbf{w}_{\perp} \equiv \mathbf{w} - \mathbf{w}_{\parallel}$, becomes particularly large for open field lines that intercept some boundaries, for example, the chamber wall in a laboratory experiment. In cases where a temperature anisotropy is sustained, i.e. $T_{\parallel} \neq T_{\perp}$ with respect to the magnetic field, the parallel heat flux \mathbf{q}_{\parallel} [1] has two components $\mathbf{q}_{\parallel} = (q_n + 2q_s)\mathbf{b}$, which are associated with the parallel and perpendicular thermal energies, respectively,

$$q_n \equiv \int m\mathbf{v}_{\parallel}^2 \mathbf{w}_{\parallel} f d^3\mathbf{v}, \quad q_s \equiv \frac{1}{2} \int m\mathbf{v}_{\perp}^2 \mathbf{w}_{\parallel} f d^3\mathbf{v}. \quad (1)$$

They modify the double-adiabatic laws (with $\partial\mathbf{B}/\partial t = 0$) as $(n^3/B^2)(d/dt)(P_{\parallel}B^2/n^3) + \nabla \cdot (q_n \mathbf{b}) - 2q_s \nabla \cdot \mathbf{b} = 0$ and $nB(d/dt)(P_{\perp}/nB) + \nabla \cdot (q_s \mathbf{b}) + q_s \nabla \cdot \mathbf{b} = 0$, with $P_{\parallel, \perp} = nT_{\parallel, \perp}$ and n the plasma density [1, 2].

Normally \mathbf{q}_{\parallel} is modeled as thermal conduction, $\mathbf{q}_{\parallel} = -\kappa_{\parallel} \nabla_{\parallel} T$, with the conductivity $\kappa_{\parallel} > 0$, so heat flows from high to low temperature region [3]. In the collisional regime where the plasma stays close to local thermodynamic equilibrium, the thermodynamic cross terms can also drive parallel heat flux by, for example, density gradient, where the transport coefficients are known to satisfy the Onsager relation [4–6]. The opposite limit of low collisionality or long mean-free-path (λ_{mfp}) is prevalent for space/astrophysical plasmas and laboratory confinement experiments. The naive approach of $\kappa_{\parallel} = \lambda_{\text{mfp}}^2 / \tau_{\text{collision}} = v_{\text{th}}^2 \tau_{\text{collision}}$ indicates enormous electron thermal conductivity which implies a flattened parallel temperature profile (subject to flux limiting in practice [7]). A more refined description (for example, by Hammett and Perkins [8] and Hazeltine [9]) illustrates the non-local nature of the parallel heat flux, $q(x) = (n_0 v_{\text{th}} / \pi^{3/2} T_0) \int_0^{\infty} [T(x-x') - T(x+x')] / x' dx'$, which still produces a heat flux that relaxes temperature gradient for monotonic temperature profile, but depends

on the global as opposed to local temperature variation. The nonlocal nature of heat flux in long λ_{mfp} plasmas has been widely studied both as a fundamental closure issue [10] and as a novel physics model for interpreting experiments [11]. It also motivates sophisticated computational method development [12]. The Hammett-Perkins-Hazeltine expression of nonlocal parallel heat flux [8, 9] is for near-Maxwellian plasmas, which is a suitable description for plasmas confined by closed flux surfaces. The open magnetic field line tends to produce significant deviation from local Maxwellian and introduce additional novel behavior for the parallel heat flux.

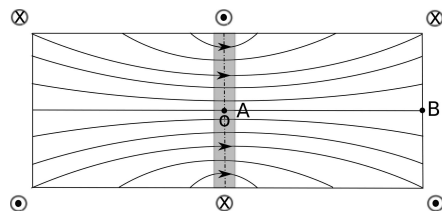


FIG. 1: Simulation setup: a symmetric flux expander is generated by current wires with B_0 (at point O) / B_w (at point B) = 5. The simulation domain has $x \in [-L_x, L_x]$ in the horizontal direction and $y \in [-L_y, L_y]$ in the vertical direction. The plasma is uniform in the z direction (out of plane) and symmetric about $x = 0$.

In this Letter, we elucidate the physics underlying a surprising but representative kinetic-Maxwell simulation result that for an open field line plasma bounded by absorbing walls, a parallel heat flux, specifically the q_n component, flows from low to high T_{\parallel} region. This contradicts the conventional thermal conduction picture and presents an interesting theoretical challenge with profound practical implications in that the parallel heat flux has a deciding role in determining the plasma profile along the open magnetic field lines. Through an analysis of the particle orbit under the combined effect of the mirror force and the ambipolar electric field in a magnetic flux expander, we find that this peculiar behavior of the parallel heat flux component q_n can be understood from the passing particle distribution functions calculated from the steady state drift-kinetic equation with

the same upstream source in the simulation. Our calculation re-affirms Hazeltine's important observation [9] that the source and wall condition enter explicitly in the parallel heat flux.

The simulation case as shown in Fig. 1, captures the essential features of a long λ_{mfp} plasma in an open magnetic field with significant $\|\mathbf{B}\|$ variation. A (quasi)-steady state is established by an upstream source compensating the wall loss, which enters the kinetic equation as

$$\frac{\partial f}{\partial t} + \mathbf{v} \cdot \frac{\partial f}{\partial \mathbf{x}} + \frac{q}{m} (\mathbf{E} + \frac{\mathbf{v}}{c} \times \mathbf{B}) \cdot \frac{\partial f}{\partial \mathbf{v}} = C(f) + S, \quad (2)$$

where the subscripts for different species are suppressed, and the source distribution is assumed to be Maxwellian,

$$S(\mathbf{x}, \mathbf{v}) = h(\mathbf{x}) \left(\frac{m}{2\pi T_s} \right)^{3/2} \exp\left(-\frac{mv^2}{2T_s}\right). \quad (3)$$

Here m is the particle mass, $T_s (= 1)$ is the source temperature, and $h(\mathbf{x})$ is the spatial distribution of the source, which is uniform and localized in the shaded region, $x \in [-L_s/2, L_s/2]$. The VPIC [13] kinetic simulation runs use a time step $\Delta t < 1/\omega_{pe}$, grid size $\Delta x = \lambda_d/4$, $L_x = 2L_y = 60\lambda_d$, $\rho_e = 4\lambda_d$ and $m_i/m_e = 100$, with λ_d , ω_{pe} and ρ_e the Debye length, the electron plasma frequency and the electron gyro-radius, respectively.

Our kinetic simulations produce quasi-steady state plasmas even in the collisionless limit [$C(f) = 0$]. As shown in Fig. 2 and 3, both ions and electrons see a large temperature anisotropy, especially in the high field region away from the absorbing boundary. The profile variation is plotted from A to B minus the Debye sheath shown in Fig. 1. Both the ion and electron perpendicular temperatures decrease toward the wall, consistent with the magnetic moment conservation in a flux expander. The parallel temperature mostly increases toward the wall as the ion and electron go down the magnetic hill. Both components of the parallel heat flux are positive which means they flow toward the wall. The q_n components, which are related to parallel thermal energy and defined in Eq. (1), are found to flow from low T_{\parallel} to high T_{\parallel} along the open magnetic field line. To understand this unusual behavior, we perform analytical calculations of the parallel heat flux and compare them to the simulation. In the limit of small ion gyroradius ρ_i over system scale L and low frequency, Eq. (2) can be reduced to the drift-kinetic equation. To lowest order in ρ_i/L , parallel streaming dominates and the steady state guiding center distribution function [14] is given by,

$$v_{\parallel} (\partial/\partial l) f(l, \epsilon, \mu, \sigma) = S(l, \epsilon, \mu), \quad (4)$$

where l is the distance along the field line so $\mathbf{b} \cdot \nabla \equiv \partial/\partial l$, $\mu = mv_{\perp}^2/2B$ is the magnetic moment, $\epsilon = mv_{\parallel}^2/2 + \mu B + q\phi_0$ is the total energy, $\sigma = \pm 1$ is positive/negative if the particle moves to the right/left, $v_{\parallel} = \sqrt{2(\epsilon - \mu B - q\phi_0)/m}$ is the guiding center speed

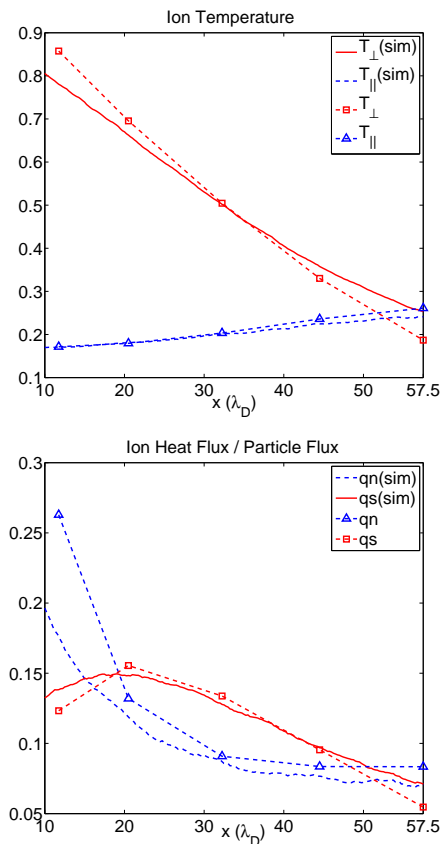


FIG. 2: Top: the ion temperature profile from simulation and analytical result; Bottom: the ion parallel heat flux from simulation and analytical result.

along the field line, ϕ_0 is the ambipolar potential. We will use $\phi_0(l)$ from the kinetic simulation in Eq. (4). Without loss of generality, ϕ_0 is set to zero at $l = 0$.

Conservation of ϵ and μ helps the classification of particle orbit. The combined force of mirror field and ambipolar electric field can be conveniently described by an effective potential $\phi_{\text{eff}}(l) = \phi_0(l) + \mu B(l)/q$. We first note that going down a magnetic hill, the ambipolar potential decreases to slow down the electrons. The ion ϕ_{eff} thus monotonically decreases toward the wall, so all ions are passing particles. For its negative charge, the electron ϕ_{eff} produces both trapped and passing orbits for different values of μ . The electron distribution can be separated into the trapped and passing population: $f_e = f_t + f_p$. The trap-passing boundary is given by an eclipse in the $(v_{\parallel}, v_{\perp})$ space,

$$v_{\parallel}^2 + v_{\perp}^2 (1 - B_w/B) = 2e(\phi - \phi_w)/m_e, \quad (5)$$

with ϕ_w the wall potential. Since all passing particles originate at the source region with non-negative parallel kinetic energy, there is another constraint in $(v_{\parallel}, v_{\perp})$,

$$v_{\parallel}^2 - v_{\perp}^2 (B_0/B - 1) + 2q\phi/m \geq 0, \quad (6)$$

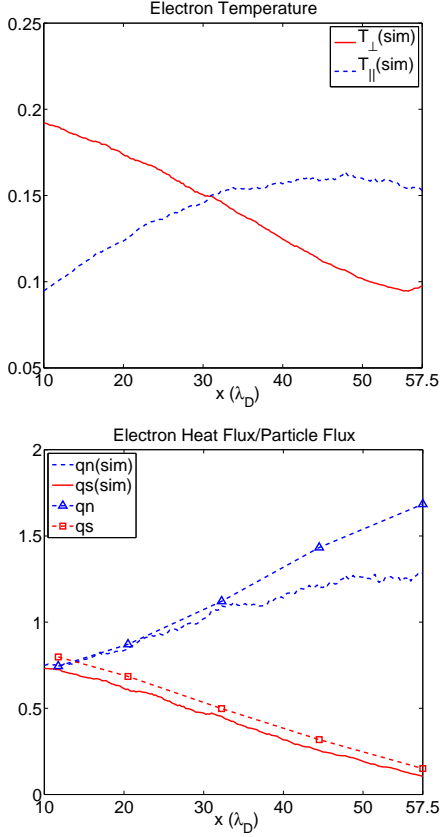


FIG. 3: Top: the electron temperature profile from simulation; Bottom: the electron parallel heat flux from simulation and analytical result.

which is bounded by a hyperbola. The particle distributions of ions and electrons from the kinetic simulation are shown in Fig. 4, along with the two constraint curves defined by Eqs. (5) (dashed thick line) and (6) (solid thick line). The particles from the source should all fall below the hyperbola, Eq. (6), and the trapped electrons are within the eclipse, Eq. (5). Due to the collisionless scattering process, such as the wave-particle interaction, there are particle fluxes across these boundaries in the velocity space, which lead to particle distribution in the inaccessible regions as shown in Fig. 4.

Only the passing particles carry energy flux to the absorbing boundary. Their distribution function is subject to the boundary condition, $f_p(-L_x, +) = f_p(+L_x, -) = 0$, where $+/-$ means particles moving to the right/left. Integrating Eq. (4) from $-L_x$ to l [14, 15], we find that the passing particles moving to the right has the distribution

$$\begin{aligned} f_p(l > 0, +) &= \int_{-L_x}^l S(s, \epsilon, \mu, +) v_{\parallel}^{-1} ds \\ &= \Gamma_s \left(\frac{m}{2\pi T_s} \right)^{3/2} \frac{\exp(-\epsilon/T_s)}{\sqrt{2(\epsilon - \mu B_0)/m}}, \end{aligned} \quad (7)$$

where $h(s) = \Gamma_s \delta(s)$ for simplicity and Γ_s corresponds to injected particle flux. The result for passing particles moving to the left is the same. The denominator in Eq. (7) implies $\epsilon \geq \mu B_0$, as in Eq. (6). The moments of the distribution function, $\langle \mathcal{A} \rangle = \int \mathcal{A} (2\pi B/m^2 v_{\parallel}) (f_p + f_t) d\epsilon d\mu = \langle \mathcal{A} \rangle_p + \langle \mathcal{A} \rangle_t$, generally have contributions from both the passing and trapped population. But the odd order moments in v_{\parallel} vanish for the trapped population due to the symmetry $f_t(\epsilon, \mu, +) = f_t(\epsilon, \mu, -)$. For example the two components of the parallel energy flux are $\frac{1}{2} \langle m v_{\parallel}^3 \rangle = \frac{1}{2} \langle m v_{\parallel}^3 \rangle_p$ and $\langle \mu B v_{\parallel} \rangle = \langle \mu B v_{\parallel} \rangle_p$.

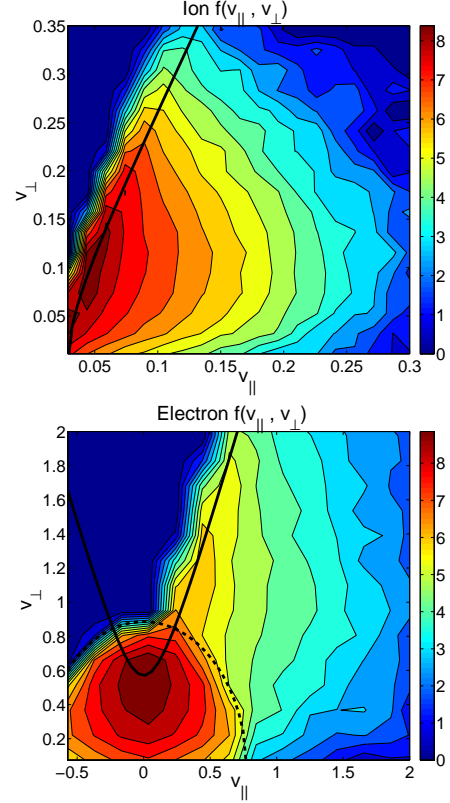


FIG. 4: The ion and electron distribution contour ($\ln(f_{i,e} + 1)$) at $l = 15\lambda_d$ (along AB in Fig. 1) from the kinetic simulation.

For ions, the integration boundary in the (μ, ϵ) space is given by the constraint $\epsilon \geq \mu B_0$. The ion density follows $n_i = \Gamma_s \sqrt{\frac{m_i}{2\pi T_s}} e^{-\frac{q\phi}{2T_s}} \int_0^{\infty} e^{-(R+1)t'} K_0(Rt' - t' - \frac{q\phi}{2T_s}) dt'$, where $R = B_0/B$, and $K_0(x)$ is the modified Bessel function of the second kind. The ion flux, $\Gamma_i \equiv n_i u_i$, is found to be proportional to the magnetic strength B , $\Gamma_i = \Gamma_s/2R = \Gamma_s B/2B_0$, consistent with the continuity equation $\nabla \cdot (\Gamma_i \vec{b}) = 0$. The parallel ion energy flux has

$$\frac{1}{2} \langle m_i v_{i\parallel}^3 \rangle = \frac{\Gamma_s T_s}{2R} \left(\frac{3}{2} - \frac{1}{R} - \frac{q\phi}{T_s} \right), \quad (8)$$

$$\langle \mu_i B v_{i\parallel} \rangle = \frac{\Gamma_s T_s}{2R^2}. \quad (9)$$

Hence the two components of ion parallel heat flux are

$q_{in} = \langle m_i v_{\parallel i}^3 \rangle - 3n_i u_i T_{i\parallel} - n_i m_i u_i^3$, and $q_{is} = \langle \mu_i B v_{\parallel i} \rangle - n_i u_i T_{i\perp}$. The expressions for the anisotropic temperatures $T_{i\parallel}$ and $T_{i\perp}$ are similarly obtained, but are not explicitly shown here. Plugging in the ambipolar potential ϕ_0 from the kinetic simulation, the analytical expressions for both ion temperatures and parallel heat fluxes are found to agree with the simulation result, as shown in Fig. 2. The ion distribution function in Eq. (7) reproduces the q_{in} that flows from low $T_{i\parallel}$ to high $T_{i\parallel}$ along the open field line.

For electrons, the trap-passing boundary must be taken into account. The above approach still holds but the integration bounds in the (μ, ϵ) space are now defined by both Eq. (5) and Eq. (6). The integration over ϵ and μ breaks into two parts. When $\mu \geq \mu_0$, it is $\epsilon \geq \mu B_0$; when $\mu < \mu_0$, it is $\epsilon \geq (\mu B_w - e\phi_w)$, where $\mu_0 = |e\phi_w|/(B_0 - B_w)$ is given by the intersection of the two constraint curves. Here, we have assumed $|\phi| < |\phi_w|(B_0 - B)/(B_0 - B_w)$, which guarantees that the electrons will be lost if they satisfy $\epsilon \geq (\mu B_w - e\phi_w)$.

The passing electron distribution, Eq.(7), uniquely determines the odd order moments, *i.e.* the parallel particle and energy fluxes. The electron particle flux is $\Gamma_e = \langle v_{\parallel} \rangle = (\Gamma_s/2R)[\text{erfc}(\sqrt{\tilde{\phi}_w}) + \alpha C \text{erfi}(\sqrt{\alpha\tilde{\phi}_w})]$, where $\alpha \equiv B_w/(B_0 - B_w)$, $\tilde{\phi}_w \equiv e|\phi_w|/T_s$, $C \equiv e^{-(\alpha+1)\tilde{\phi}_w}/\alpha^{3/2}$ and $\text{erf}()$, $\text{erfi}()$, $\text{erfc}()$ are the standard, imaginary, and complementary error functions. Comparing the particle flux of the two species with $\tilde{\phi}_w = 0.241 T_s$ from the simulation, we find $\Gamma_{ep}/\Gamma_i \approx 0.9$, which implies that the collisionless detrapping of the trapped electron population makes a small but essential (to maintain ambipolarity) contribution to the total electron flux to the wall.

The two components of the electron parallel energy flux are similarly integrated,

$$\begin{aligned} \frac{1}{2}\langle m_e v_{e\parallel}^3 \rangle &= \frac{\Gamma_s T_s}{2R^2} \left[D + R \left(\frac{3}{2} - \frac{1}{R} + \frac{e\phi}{T_s} \right) \text{erfc}(\sqrt{\tilde{\phi}_w}) \right. \\ &\quad \left. + C \left(R\alpha \frac{e\phi}{T_s} + RG - G - \frac{1}{2} \right) \text{erfi}(\sqrt{\alpha\tilde{\phi}_w}) \right], \\ \langle \mu_e B v_{e\parallel} \rangle &= \frac{\Gamma_s T_s}{2R^2} \left[-D + \text{erfc}(\sqrt{\tilde{\phi}_w}) \right. \\ &\quad \left. + C \left(G + \frac{1}{2} \right) \text{erfi}(\sqrt{\alpha\tilde{\phi}_w}) \right], \end{aligned} \quad (10)$$

where $D \equiv e^{-\tilde{\phi}_w} \sqrt{\tilde{\phi}_w/\pi} (1 + \alpha)/\alpha$, $G \equiv \alpha[3/2 + (1 + \alpha)\tilde{\phi}_w]$. The electron parallel heat flux is again obtained by subtracting the convective energy flux as for the ion, but the $n_e m_e u_e^3$ term is ignorable for $m_i/m_e \gg 1$. Since we do not have an analytical expression for the trapped electron distribution, the convective pieces $n_e u_e T_{e\parallel}$ and $n_e u_e T_{e\perp}$ are substituted by $\Gamma_e T_{e\parallel}$ and $\Gamma_e T_{e\perp}$ with $T_{e\parallel, \perp}$ directly from the simulation. The resulting q_{en} and q_{es} compare favorably with those directly measured in the simulation, as shown in Fig. 3. Again the q_{en} flows from low $T_{e\parallel}$ to high $T_{e\parallel}$ along the open field line.

The passing electrons, upon integrating f_p over ϵ and μ as above, make a small contribution to the total electron density $n_{ep} \sim (m_e/m_i)^{1/2} n_i$. But due to the large electron thermal speed $v_{th,e} = (m_i/m_e)^{1/2} v_{th,i}$, the passing electrons from source distribution alone, Eq.(7), dominate the ambipolar flux $\Gamma_{ep} \approx 0.9\Gamma_i$, and the parallel energy flux. The input energy flux by the source, $Q_{in} = (3/4)\Gamma_s T_s$, is the same for ions and electrons. The ambipolar electric field transfers part of the electron energy into ions. The parallel energy flux $Q = \langle m v_{\parallel}^3 \rangle_p / 2 + \langle \mu B v_{\parallel} \rangle_p$ is larger for the ions compared with the electrons ($Q_i = 1.37Q_e$). This calculation ignores the wave-particle interaction and collisionless detrapping of the electrons, but finds $Q_i + Q_e \approx 2Q_{in}$. This implies that the collisionless detrapping of the trapped electrons makes a similarly small contribution to the parallel energy flux, just as the parallel particle flux. Unlike the ions which have a much greater convective flow energy component, the electron parallel energy flux has a much greater parallel heat flux ($q_{en} + q_{es}$).

In conclusion, the novel behavior of parallel heat flux q_n flows from low to high T_{\parallel} along an open magnetic field line can be understood in terms of the passing ion and electron distribution functions going down a magnetic hill. The primary effect of the mirror force and ambipolar electric field is to compress the passing particle distribution function in v_{\perp} but broaden it in v_{\parallel} . Since plasma temperature is associated with the spreading of its distribution about the mean value, the perpendicular temperature of the passing particles decreases while the parallel temperature increases. The conductive heat flux is mathematically determined by the skewness of the distribution. For example, the ion distribution about v_{\parallel} has positive skewness and thus q_{in} is going to the wall.

We wish to thank Herb Berk for useful discussions and Department of Energy Office of Fusion Sciences for support under contract DE-AC52-06NA25396.

-
- [1] G. F. Chew, M. L. Goldberger, and F. E. Low, *Proc. R. Soc. A* **236**, 112 (1956).
- [2] A. Macmahon, *Phys. Fluids* **8**, 1840 (1965).
- [3] S. I. Braginskii, *Rev. Plasma Phys.* **1**, 205 (1965).
- [4] T. C. Luce, C. C. Petty, and J. C. M. Dehass *Phys. Rev. Lett.* **68**, 52 (1992).
- [5] A. H. Boozer, *Phys. Fluids B* **4**, 2845 (1992).
- [6] J. A. Krommes, *Phys. Fluids B* **5**, 3908 (1993).
- [7] O.V. Batishchev, et al. *Phys. Plasmas* **4**, 1672 (1997).
- [8] G. W. Hammett & F. W. Perkins, *Phys. Rev. Lett.* **64**, 3019 (1990).
- [9] R. D. Hazeltine, *Phys. Plasmas* **5**, 3282 (1998).
- [10] E. D. Held, et al, *Phys. Plasmas* **11**, 2419 (2004).
- [11] J. D. Callen & M. W. Kissick, *Plasma Phys. Control. Fusion* **39**, B173 (1997); D. del-Castillo-Negrete, et al, *Nuclear Fusion* **48**, 075009 (2008).
- [12] D. del-Castillo-Negrete & L. Chacon, *Phys. Rev. Lett.* **106**, 195004 (2011).
- [13] K. Bowers, et al. *Phys. Plasmas* **15**, 055703 (2008).
- [14] K. Sato, F. Miyawaki, and W. Fukui, *Phys. Fluids B* **1**, 725 (1989).
- [15] L. Tonks and I. Langmuir, *Phys. Rev.* **34**, 876 (1929).